nature synthesis

Article

https://doi.org/10.1038/s44160-023-00311-9

Rare earth–cobalt bimetallic catalysis mediates stereocontrolled living radical polymerization of acrylamides

Received: 11 November 2022

Accepted: 31 March 2023

Published online: 04 May 2023

Check for updates

Xiaowei Zhang [1], Fei Lin [1], Mengxue Cao [1] & Mingjiang Zhong [1,2]

The tacticity of polymers is one of the governing microstructural parameters that determines their material properties. Current methods to access stereoregular polymers are based on coordination and ionic polymerizations. However, these polymerization methods are limited to a small group of monomers. By contrast, radical polymerization is compatible with diverse chemical functionalities but provides poor stereocontrol primarily due to the challenge of controlling the stereochemistry of carbon-centred radicals. Here, by covalently tethering a rare earth cation-based Lewis acid to cobalt(III) complexes, we designed a bimetallic catalytic system to achieve stereocontrol in living radical polymerization. The interplay of pendant group–Lewis acid interaction and cobalt-mediated reversible radical deactivation within a confined space results in chain propagation through a *meso*-configurated radical chain end. Acrylamide monomers with diverse polar and ionic pendant groups were polymerized in a stereoregular manner with a percentage of *meso* diads as high as 95%. Thermo-responsive, adhesion and electrical properties of homopolymers were readily diversified by tuning tacticity without compositional variance. This method provides a diversity-oriented design platform to access polymers with broadly tunable bulk, solution and interfacial properties from single monomer feedstock through tacticity engineering.

The material properties of polymers with given chemical composition can be tuned through engineering the relative stereochemistry of repeat units, also known as tacticity[1]. Vinyl polymers with varied backbone stereoregularities exhibit different thermomechanical properties[2,3], charge carrier mobility[4], dielectric properties[5], self-assembly behaviours[6], processability[7] and gas permeability[8]. These intrinsic structure–property relationships motivated the development of stereocontrolled vinyl polymerizations to access polymer products with diversified properties from unchanged monomer feedstocks. Current stereocontrolled coordination and ionic polymerizations have been limited to a small group of vinyl monomers and demand rigorously developed reaction conditions. Radical polymerization is considered the most versatile vinyl polymerization method as a consequence of its compatibility with diverse functional groups and high tolerance to impurities, and has been industrially applied to produce commodity polymers in a broad range of reaction media, for example, aqueous and protic solutions, gas phase, emulsion and dispersion. However, development of stereocontrolled radical polymerization remains a fundamental challenge (Fig. 1a) primarily due to the difficulty in controlling the stereochemistry of the radical propagating chain ends with an sp^2-hybridized planar geometry[9,10]. The continuous generation of new stereogenic radical centres during the chain-growth polymerization process further complicates the development of stereocontrolled radical polymerization. Consequently, products containing around

[1]Department of Chemical and Environmental Engineering, Yale University, New Haven, CT, USA. [2]Department of Chemistry, Yale University, New Haven, CT, USA. e-mail: mingjiang.zhong@yale.edu

https://doi.org/10.1038/s44160-023-00311-9

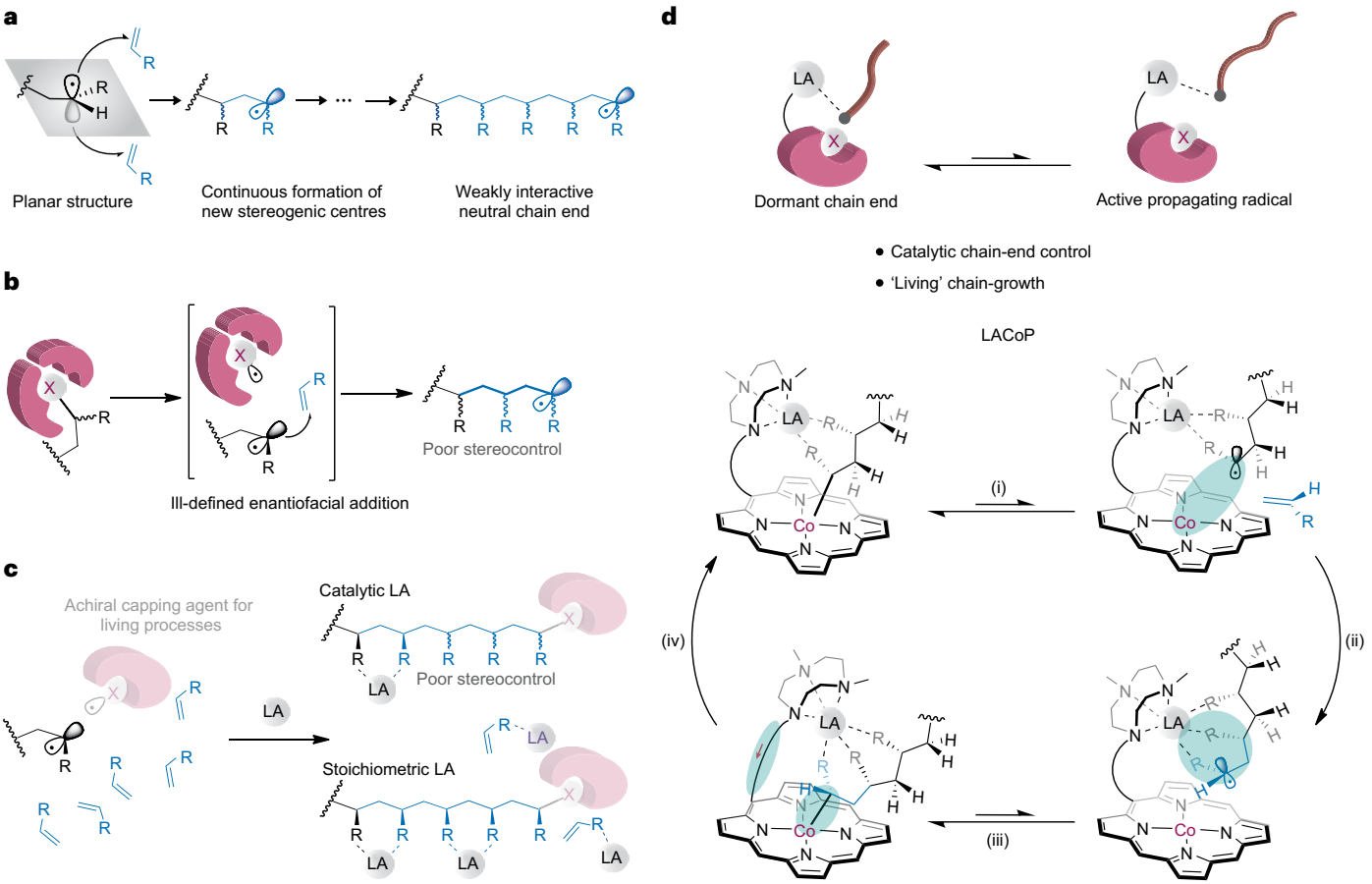

Fig. 1 | Stereocontrol in radical polymerizations. a, Challenges of stereocontrol associated with radical polymerization. **b**, Weak interaction between a chiral radical capping agent and the radical chain-end leads to negligible stereocontrol in LRP. **c**, Adding LAs of a stoichiometric amount relative to the monomer results in a certain degree of stereocontrol in radical polymerizations. **d**, From this work: the stereocontrolled LRP mediated by LACoP bimetallic catalysts; the LA is localized at propagating chain end for site-specific chelation owing to the efficient reversible radical deactivation enabled by cobalt–porphyrin, forming a *meso* diad enriched polymer chain.

50% *meso* (*m*) and *racemo* (*r*) diads, that is, atactic polymers without iso- or syndio-tacticity enrichment, are often obtained in radical polymerization.

Designing catalysts to tame a weakly interactive radical for a stereocontrolled process has been generally difficult. The enantiofacially differentiated vinyl addition enabled by organometallic bonding in coordination polymerizations[11–13] or electrostatic interaction in ionic polymerizations[14,15] cannot be easily realized in radical polymerization[16]. Radicals can be reversibly deactivated by a chain-end capping agent in living radical polymerization (LRP) techniques through which polymers with tailored molecular weight, dispersity and topology can be synthesized[17]. Capping agents with defined chirality were designed for enantioselective monomer additions (Fig. 1b). However, the weak interaction between the non-bonding neutral radical chain end and a designed chiral capping agent resulted in negligible stereocontrol[18,19].

Stereoregular polymers have been synthesized through radical polymerization of chiral auxiliary monomers[20] or in a rationally designed reaction environment, for example, in the presence of fluoroalcohols[21] or under spatial confinement[22]. Adding Lewis acid (LA) has been widely demonstrated as a more universal and scalable strategy to promote the stereocontrol in conventional radical polymerization or LRP of common vinyl monomers under readily accessible reaction conditions[23,24]. A prevalent rationale attributes this LA-enhanced stereocontrol to the hypothesis that LA binds to the polar pendant groups of the terminal and penultimate enchained monomers, thereby forming a *meso*-configuration at the adjacently chelated units on the subsequent monomer addition (Fig. 1c)[16,25]. While this strategy successfully converted the atactic polymers to isotacticity-enriched polymers (for example, more than 80% *m*) with drastically altered materials properties, extensive application of this method is restricted by the high metallic LA loading and its failure in the polymerizations of strongly chelating or ionic monomers. Typically, 10–20 mol% LA (for example, rare earth metals) relative to the monomer is required to ensure LA chelation with the pendant groups at the growing chain ends due to the presence of numerous competing chelating species including non-chain-end pendant groups of polymers and unreacted monomers. This high LA loading may also cause physical chain crosslinking and crossover reactions with pendant functionalities.

We present here a molecular design of rare earth–cobalt-based bimetallic system to enable chain-end-specific radical interaction (Fig. 1d). This system builds a foundation for the development of a catalytic approach to controlling stereochemistry in radical polymerization with minimized background interference. In our design, a multidentate cyclic ligand of aza-crown ether (ACE) that is covalently anchored with an organometallic cobalt(III)–porphyrin (R–Co^{III}–por) binds to LA, for example, rare earth cations, yielding a LA-tethered cobalt(III)–porphyrin (LACoP) bimetallic complex. The R–Co^{III}–por centre is responsible for the photocatalytic initiation and activation of a living radical chain-growth process[26] with the tethered LA confined in proximity to the growing chain end. The propagating radical R• formed from homolytic cleavage of the C–Co^{III} bond (Fig. 1d(i)) undergoes *meso*

addition to an incoming monomer due to the chain-end-selective LA chelation (Fig. 1d(ii)). The in situ generated Co^{II}–por can reversibly deactivate R• to form an R–Co^{III}–por dormant species either before or after the monomer addition (Fig. 1d(iii))[27]. The chain-end-chelated LA can direct a Co–por to regulate the growth of the same polymer chain and suppress the interchain transfer of LACoP: a competing process detrimental for the chain-end-specific interaction. Conversely, the covalently linked Co–por mediates a rapid deactivation reaction through a pseudo-intramolecular pathway, limiting the number of monomers added during each activation–deactivation cycle and further facilitating the chain-end stereocontrol. Although each monomer addition event produces a new terminal unit, the subsequent recapping of radical by Co^{II}–por forces the tethered LA to rearrange to interact with the newest enchained monomers and ensure continuous *meso* monomer additions even at catalytic loading of LA (Fig. 1d(iv)). Whereas the concept of bimetallic catalysis involving covalently bridged hetero-catalytic centres has been applied in non-radical systems to attain high-performance polymerizations[28,29], leveraging this proximity effect to realize chain-end-controlled radical propagation remains unprecedented.

Results and discussion

LACoP-mediated LRP

To prove our hypothesis, we synthesized a series of LACoPs as initiators for *N*,*N*-dimethylacrylamide (DMAA) photopolymerizations under visible light irradiation (Fig. 2a,b and Supplementary Table 6). Figure 2a summarizes the data of *meso* diad percentages obtained from LACoP-initiated polymerizations in methanol with varied loadings of lanthanum(III) trifluoromethanesulfonate ($La(OTf)_3$). The initial attempts involving **1b** with an alkylated cyclen ligand resulted in polyDMAA with 75–85% *m* when 0.5–2.5 mol% $La(OTf)_3$ was used relative to DMAA. The degree of isotacticity monotonically increased with increasing the equivalent of $La(OTf)_3$. In comparison, a lower percentage of *meso* diads (less than 70% *m*) was obtained with 2.5 mol% $La(OTf)_3$ from a conventional radical polymerization initiated by a diphenyl(2,4,6-trimethylbenzoyl)phosphine oxide (TPO) photo-initiator. An R–Co^{III}–por complex without tethered ACE (**1a**) provided up to 74% *m* at the same $La(OTf)_3$ loading. Adding non-tethered ACE into the **1a**-initiated polymerization resulted in negligible change in the stereocontrol, indicating the essential role of the covalently tethered LA in *meso* radical addition. The **1a**-enhanced isotacticity, compared to TPO-initiated radical polymerization, could be attributed to the weak LA interaction with the carboxylate group of **1a** as well as a controlled chain-growth process mediated by Co–por, and has been generally observed in many other LRP systems[30–33]. Replacing the *para*-substituted LA ligand (**1b**) with a *meta*-substituent (**1c**) with respect to the porphyrin ring provides a more appropriate bite angle of the dinuclear catalyst for a chain-end-selective chelation, and resulted in moderate isotacticity enhancement, for example, 88% *m* (**1c**) versus 85% *m* (**1b**) at a 2.5 mol% $La(OTf)_3$ loading.

Further investigation of LACoPs was centred on engineering the binding affinity and geometry of the LA ligand. A Co–por complex **1d** contains a tridentate triazacyclononane (TACN)-derived ligand with a similar LA binding constant to the tetradentate ACE[34,35]. PolyDMAA with more than 90% *m* was obtained in a **1d**-initiated polymerization with merely 2.5 mol% $La(OTf)_3$ added, although a similar level of isotacticity could not be realized in TPO-initiated radical polymerization with more than 10% LA added (Supplementary Table 6). The percentage of *meso*–*meso* triads (*mm*) in the polyDMAA with 95% *m* was quantified to be 90% *mm* according to its clearly distinguishable chemical shifts in the proton nuclear magnetic resonance (^{1}H-NMR) spectrum (Supplementary Fig. 42). This improved stereocontrol compared to **1c** plausibly originated from the enhanced interactions of **1d** with chain-end pendants due to its reduced ligand cone angle and coordination number. By contrast, **1e** resulted in poor stereocontrol due to the weak *N*-monosubstituted crown ether ligand with a binding constant roughly eight orders of magnitude lower than cyclen[36]. In addition to the ligand design, selecting appropriate LA could be equally critical to the stereocontrol, especially in a reaction medium rich in competing chelating species. In the proposed mechanism, at least two coordination sites of LA need to be reserved for the chelation with chain-end pendant groups in a *meso* radical addition. Among a series of LAs we screened (Supplementary Table 4), rare earth metal cations with a large coordination number, particularly lanthanum(III) (La^{3+}) and yttrium(III) (Y^{3+}), presented superior stereocontrol.

The scope of monomers was expanded to acrylamides with various *N*-substituents (Fig. 2c). **1d**-Initiated polymerizations generated polymers with a higher isotacticity compared to TPO-initiated polymerizations from all monomers. Alkyl-substituted acrylamides including *N*,*N*-diethylacrylamide (**2b**, DEAA) and *N*-isopropylacrylamide (**2c**, NIPAM) provided more than 90% *m* in **1d**-initiated polymerizations with addition of 5 mol% $La(OTf)_3$. A wide range of polar pendants were well-tolerated, including ether, amine, alcohol and cation. Polymerizations of **2d**–**g** resulted in polymers with up to 85% *m*, slightly lower than those alkyl-substituted acrylamides due to the competitive coordination interactions of the pendant ether groups. *N*-(3-(dimethylamino)propyl)acrylamide (**2 h**) and *N*-(2-hydroxyethyl) acrylamide (**2i**, HEAA) that seem compatible only with radical polymerization were isotactically polymerized using **1d**, although TPO-initiated radical polymerizations provided poor stereocontrol even at elevated LA loading and resulted in insoluble products possibly due to the abovementioned physical crosslinking. Positively charged polymers with nearly 80% *m* were synthesized from (3-acrylamidopropyl)trimethylammonium trifluoromethanesulfonate (**2j**, APTMAT). As a controlled experiment, introducing a strongly coordinating group that interferes the ACE complexation with La^{3+}, for example, sulfonate in **2k**, diminished the isotacticity enrichment, further revealing that covalently tethering LA to the radical deactivator is key to the stereocontrol attained in LACoP-mediated LRP.

The crystallinity and related thermal properties of tacticity-varied polyDMAA (NMR spectra shown in Fig. 2d) were characterized by differential scanning calorimetry (DSC) and wide-angle X-ray scattering (WAXS). An isotactic polyDMAA (95% *m*) exhibited a glass transition temperature (T_g) of 109 °C, 20 °C lower than its atactic counterpart with 51% *m* (Fig. 2e). Consistent with previous studies[30], first-order phase transition absent in the atactic sample was observed in the DSC heating curve of the 95% *m* polyDMAA with an exothermic crystallization peak at T_c of 177 °C and an endothermic melting peak at T_m of 258 °C, suggesting the formation of a semicrystalline structure. Decreasing the degree of isotacticity from 95% *m* to 83% *m* reduced the specific enthalpy change of melting from 16.7 to 5.6 J g^{-1} due to the decreased fraction of crystalline phase. Sharp and intensive diffractions originating from the crystalline phase were observed in WAXS profiles of the two isotacticity-enriched polyDMAAs (Fig. 2f).

Mechanistic investigation

The characteristics of a living chain-growth process were probed in the **1d**-initiated polymerizations of DMAA. Instantaneous quenching of the polymerization on either addition of a nitroxide radical or removal of light irradiation (Supplementary Information) validated the radical-mediated polymerization mechanism in the presence of LA. The pseudo-first-order polymerization kinetics (Fig. 3a) resulted in narrowly distributed molecular weight (dispersity index $Đ < 1.3$) that grew linearly with monomer consumption (Fig. 3b). The deviation of the molecular weight from a theoretical value originated from the relatively low initiation efficiency due to a larger bond dissociation free energy of the Co–carbonyl bond of the initiator than the Co–C bond at the polyacrylamide chain end (Supplementary Table 21). LACoPs with a more labile Co–C bond could potentially be designed to further improve the control over both molecular weight and tacticity.

https://doi.org/10.1038/s44160-023-00311-9

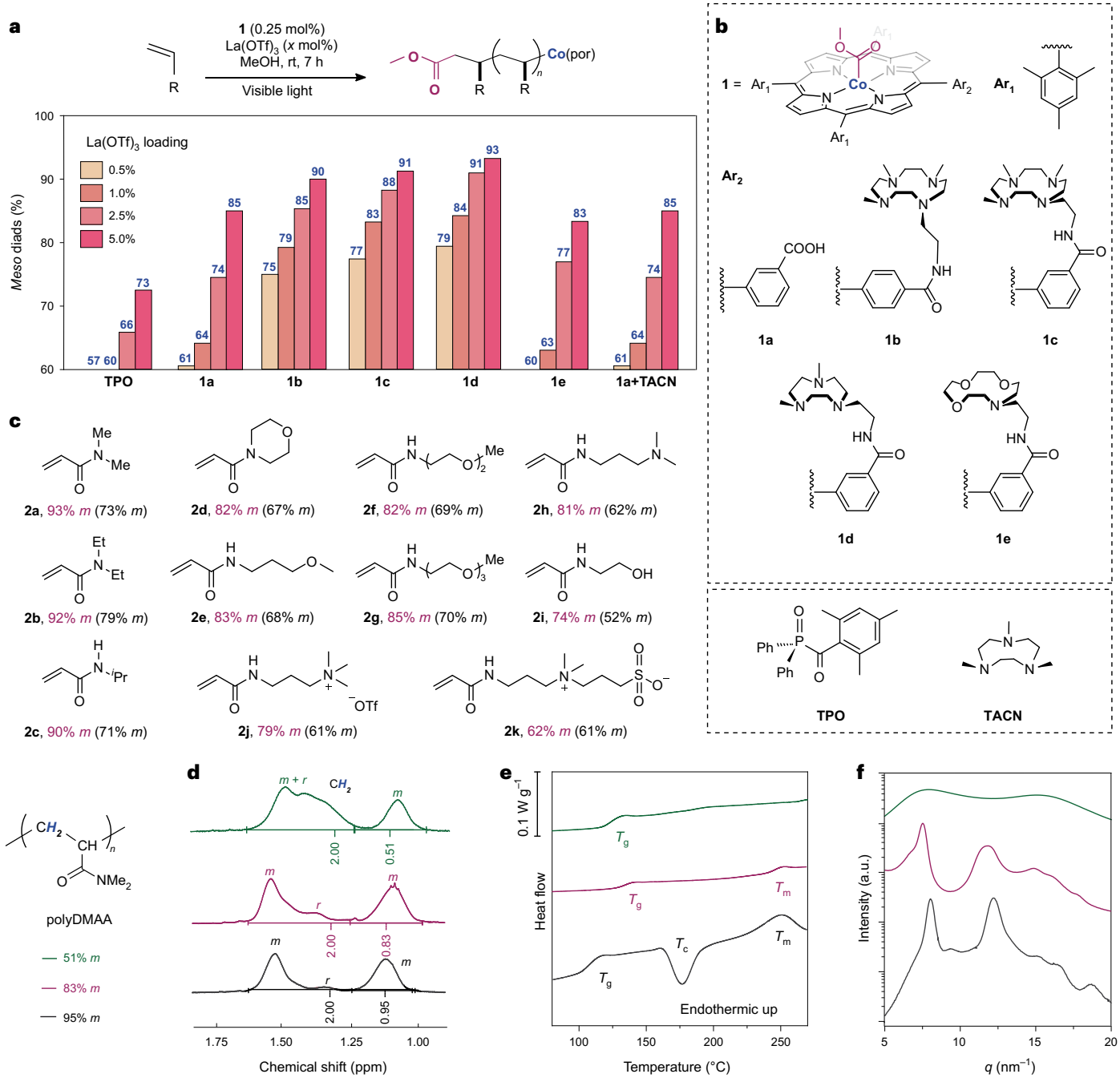

Fig. 2 | LACoP-mediated LRPs in methanol. a, General scheme and tacticity data of LACoP-initiated photopolymerization of acrylamides. $[DMAA]_0$:$[initiator]_0$ = 400:1. rt, room temperature. **b**, Chemical structures of initiators and ligands used in the studies. **c**, Scope of monomers and corresponding *meso* diad percentages obtained from polymerizations initiated by **1d** (red) and TPO (black) with 5 mol% $La(OTf)_3$. **d**, ^{1}H-NMR spectra used to quantify the composition of *meso* and/or *racemo* diads. **e**,**f**, PolyDMAA with varied degrees of tacticity displayed different phase transition behaviours and levels of crystallinity as reflected by DSC curves (**e**) and WAXS profiles (**f**).

The livingness rendered by the Co–por-mediated reversible radical deactivation was evidenced by the successful synthesis of polyDMAA-containing block copolymers. An isotactic polyDMAA macroinitiator end-functionalized with Co^{III}–por was synthesized and isolated from a **1d**-initiated polymerization. The clear shift of the gel permeation chromatography (GPC) trace (Fig. 3c) after its chain extension with *tert*-butyl acrylate suggested a high chain-end fidelity preserved in a living chain-growth process. This stereocontrolled LRP also opened a way to the one-pot synthesis of stereo-block polyacrylamides containing an atactic and an isotactic block by injecting LA solution to LACoP-mediated homopolymerizations at a given time (Supplementary Information).

Comparison of the kinetic characteristics under dissimilar reaction conditions provided mechanistic insights into the LACoP-mediated LRP. LA-accelerated polymerization that occurs in conventional radical polymerization[37] was also observed in LACoP-mediated LRP (Fig. 3d). This acceleration at an unchanged radical concentration could be ascribed to the LA-enhanced reactivity of propagating radicals[16], which is in agreement with the postulated *meso* radical addition enabled by a chain-end-specific interaction with LA. LA-induced

https://doi.org/10.1038/s44160-023-00311-9

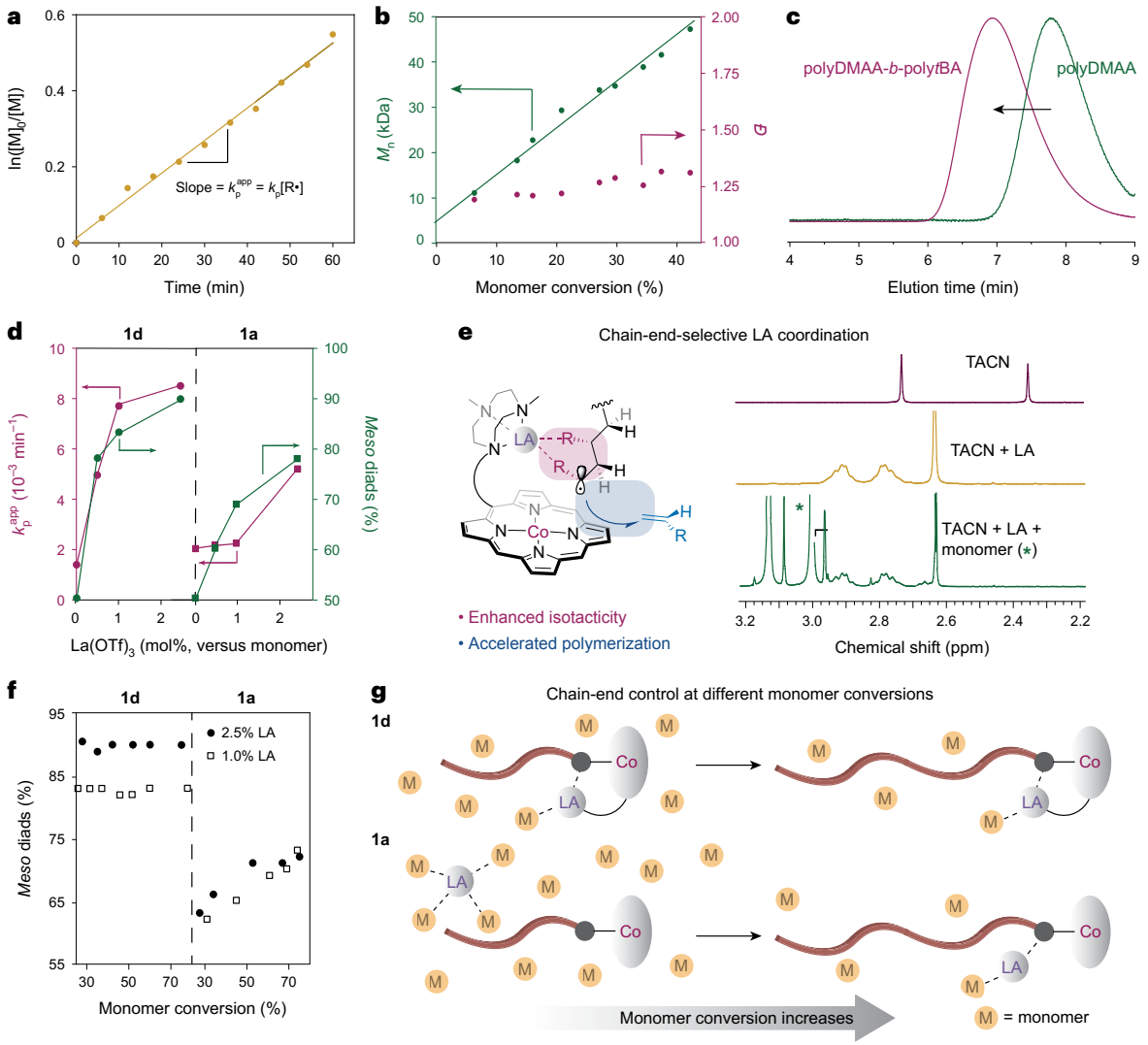

Fig. 3 | Kinetic and mechanistic studies of LACoP-mediated LRPs. **a**,**b**, Semilogarithmic pseudo-first-order kinetic plot (**a**) and evolution of molecular weight and dispersity (**b**) for the polymerization of DMAA at 2.5% $La(OTf)_3$ loading and $[DMAA]_0$:$[\mathbf{1d}]_0$ = 400:1. **c**, GPC traces before and after chain extension of a polyDMAA macroinitiator with *tert*-butyl acrylate. **d**, Apparent propagation rate coefficients and *meso* diad percentages in **1d**- and **1a**-initiated LRPs. **e**, Schematic description of chain-end-selective LA coordination in **1d**-initiated polymerization and ^{1}H-NMR studies of LA or TACN coordination. **f**, Plot of *meso* diad percentage versus DMAA conversion. **g**, Proposed mechanisms of **1d**- and **1a**-initiated LRPs at different monomer conversions.

acceleration in the LACoP-mediated LRP was investigated by relating both the apparent propagation rate coefficient (k_p^{app}) and degree of isotacticity with the $La(OTf)_3$ loading (Fig. 3d and Supplementary Table 10). In **1d**-initiated LRPs, a sharp increase of k_p^{app} and isotacticity was obtained below 1 mol% $La(OTf)_3$. When **1a** with weak LA chelation was used, $La(OTf)_3$ resulted in little impact on k_p^{app} and poorer stereocontrol until its loading reached 2.5 mol%. For further comparison, a k_p^{app} of 5.0×10^{-3} min^{-1} with 78% *m* was achieved using **1d** and only 0.5 mol% $La(OTf)_3$, while 2.5 mol% LA was needed in the **1a**-initiated LRP to obtain a similar level of acceleration ($k_p^{app} = 5.4 \times 10^{-3}$ min^{-1}) and isotacticity (77% *m*). The remarkable acceleration accompanied with a more prominent isotacticity enhancement in **1d**-initiated LRP demonstrated that the covalently attached ACE facilitated the chain-end-specific LA chelation that is beneficial for both fast kinetics and *meso* radical addition.

^{1}H-NMR spectroscopic studies revealed that LA coordinated preferentially with ACE over monomer and solvent. The almost identical NMR spectra of a La^{3+}–TACN methanol-d_4 solution before and after adding DMAA monomers (Fig. 3e and Supplementary Fig. 7) indicated stable La^{3+}–TACN complexation at a polymerization-relevant stoichiometry. It is worthwhile noting that methanol appeared to be an optimal solvent for the polymerization (Supplementary Table 1) not solely because of its excellent solubility for all reaction species but also a stereocontrol-beneficial LA coordination behaviour as demonstrated in previous work (Supplementary Figs. 15 and 16 and Supplementary Table 11)[38]. The good compatibility of LACoP with a protic environment allowed a stereocontrolled LRP of DMAA (roughly 90% *m*) in the presence of up to 2.5% water by volume (Supplementary Figs. 25 and 26).

The quality of stereocontrol can be improved by suppressing other LA-chelating species that compete with the chain-end chelation. Therefore, in conventional radical polymerization[39,40] and **1a**-initiated LRP the degree of isotacticity changed with the progressive consumption of monomers due to the difference in binding strengths of monomer and polymer with LA. The conversion-independent isotacticity in **1d**-initiated LRP (Fig. 3f) is consistent with the proposed LACoP-enabled stereocontrol; LA is selectively chelated by the pendant groups located at the radical chain end throughout the entire polymerization

https://doi.org/10.1038/s44160-023-00311-9

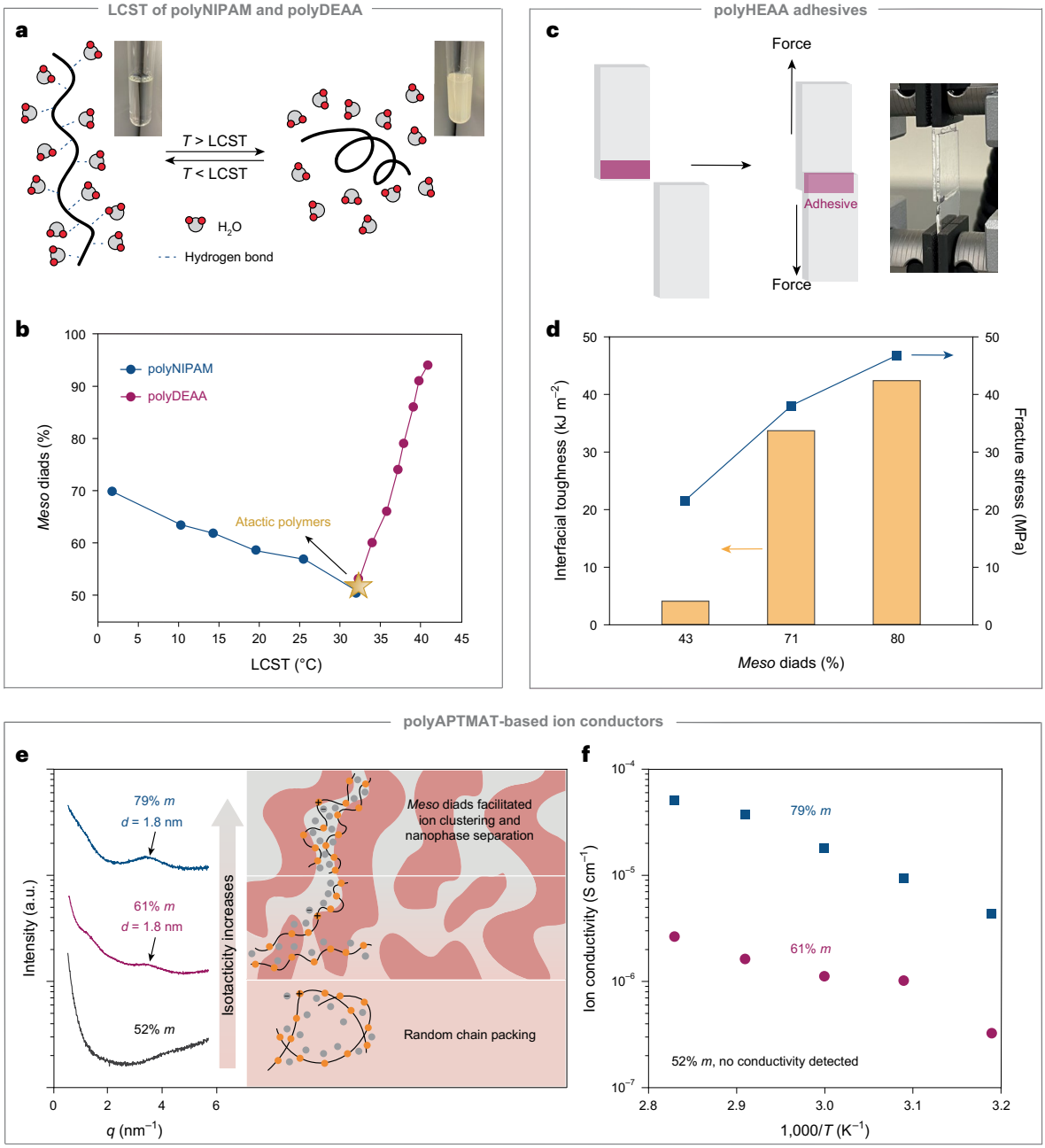

Fig. 4 | Tacticity-dependent material properties. a,**b**, Schematic illustration of LCST behaviour (**a**) and the opposing LCST dependences of polyDEAA and polyNIPAM on the degree of isotacticity (**b**). **c**,**d**, Experimental setup for adhesion evaluation of polyHEAA (**c**) and summarized data suggesting that the interfacial toughness and fracture stress are both increasing functions of isotacticity (**d**). **e**,**f**, Isotacticity-induced nanophase separation of bulk polyAPTMAT, evidenced by WAXS profiles (**e**), creates nanochannels for ion conduction that can be quantitatively accessed by electrochemical impedance spectroscopy (**f**).

(Fig. 3g). This mechanism, based on chain-end-specific interaction, was corroborated with the diad and triad composition analysis on the basis of Markovian statistics (Supplementary Information)[41].

Tacticity-dependent material properties

The stereocontrolled LRP provides an ideal platform for the preparation of well-defined polymers for systematic and accurate assessment of the tacticity influence on polymer properties. This outcome enables facile diversification of polymer properties in solution, interface and bulk states through tacticity engineering. Thermo-responsive polymers are widely used in biomedical engineering[42] and design of smart devices[43]. The thermo-responsiveness of commonly studied polyacrylamides, for example, polyDEAA and polyNIPAM, are captured by their lower critical solution temperature (LCST) above which a dissolved polymer becomes insoluble in water (Fig. 4a). Atactic polyDEAA and polyNIPAM share a mutual LCST around 33 ± 1 °C (ref. 44). Such single-point LCST limits their broader applications and is often adjusted by integrating comonomers[45–47]. Nevertheless, this copolymerization strategy lacks robust predictability and reproducibility due to the unclearly defined monomer sequence as well as the underexplored effects of molecular weight and composition on LCST. Herein, we accessed a notably expanded tuning window of LCST by varying the degree of isotacticity. LCST increased with increasing isotacticity of polyDEAA (Fig. 4b, red branch, and Supplementary Fig. 23), plausibly due to the enhanced hydrophilicity through cooperative hydrogen bond interactions between the *meso*-configurated neighbouring units

and a water molecule[48]. When the percentage of *meso* diads changed from 66% *m* to 94% *m*, the LCST increased from 35.8 to 40.9 °C. Overall, a continuous change of LCST from 33 to 42 °C was achieved in homopolymerized DEAA without compositional variance. The LCST was found to be independent of molecular weight and concentration of polyDEAA (Supplementary Figs. 18 and 19) under the studied conditions. Thus, a one-to-one correspondence was constructed between the degree of isotacticity and LCST. Different from polyDEAA solutions in which tacticity primarily influences the hydration of polymer solutes, the *meso* pendant units of polyNIPAM also greatly enhance the intra-/intermolecular interaction contributed by the dehydrating hydrogen bonds between amide groups and therefore increase the hydrophobicity of the polymers[49–51]. Collectively, the LCST of polyNIPAM displayed an opposite but more profound tacticity-dependence (Fig. 4b, blue branch and Supplementary Fig. 26). The aqueous solution of polyNIPAM with 54% *m* became cloudy at 25.5 °C and further increasing to 70% *m* resulted in a sub-room temperature thermo-response at 1.5 °C. The two different tacticity-dependences complementarily provide tunable LCST from 0 to 43 °C, broadly covering the temperature range relevant to biomedical and responsive device applications.

A further attempt towards property diversification was focused on the interfacial adhesion behaviours of polyHEAA, the atactic forms and analogues of which have demonstrated promise as (bio-)adhesives[52,53]. Lap shear tests were carried out using glass slides adhered with isotacticity-varied polyHEAA samples plasticized with the same fraction of glycerol (Fig. 4c). While the adhesion abilities of all polyHEAA samples were quantified to be within the anticipated window of commercial adhesives (Supplementary Fig. 37), both failure shear stress and interfacial toughness monotonically increased with respect to the degree of isotacticity (Fig. 4d and Supplementary Table 18). PolyHEAA with 80% *m* cost more than ten times the energy than polyHEAA with 43% *m* to unbond the single-lap joint. The isotacticity-enhanced adhesion achieved without changes in chemical composition was due to the *meso*-configurated neighbouring hydroxy pendants that provided uniformly oriented hydrogen bonds to cooperatively adhere the glass surface[54].

Design of high-performance solid-state polyelectrolytes is of high industrial value in battery, sensor and ion-exchange membrane applications[55–57]. The conventional strategy of introducing additives into polyelectrolyte to enhance ion conductivity often compromises other critical material properties such as processability, durability, as well as the solid-state nature[58]. Here, we demonstrate an additive-free method to enhance ion conductivity of bulk polyAPTMAT that consists of a polycation backbone and mobile counter anions. Three viscoelastic solids of polyAPTMAT were prepared with adjusted tacticity through LACoP-mediated LRP. The heterogeneous phase with a correlation length of 1.8 nm observed in isotacticity-enriched samples (Fig. 4e) indicated that the *meso*-configurated pendants induced ion clustering due to increased local ion density[59,60], resulting in phase segregation between backbone and ionic pendants. The conductivity of atactic polyAPTMAT with randomly packed chains was below the detection limit of the used electrochemical impendence spectroscopy method. However, ion conductivity in the range of 10^{-7}–10^{-4} S cm^{-1} was obtained in isotacticity-enriched samples (Supplementary Figs. 32 and 33). PolyAPTMAT with 79% *meso* diads displayed a more intense scattering peak and provided ion conductivity over one order of magnitude higher than that with 61% *meso* diads, suggesting that the formed nanophase-separated structures provided conducting channels for the charge carriers and reduced the energetic barrier of the anion transport.

Conclusions

In summary, we designed a rare earth–cobalt bimetallic catalytic system to realize stereocontrolled LRPs. Polyacrylamides with diversified properties were readily prepared by varying their main chain stereoregularity. We anticipate that the dinuclear molecular catalyst design can be extended to a variety of stereocontrolled polymerizations. Knowledge attained from studies of small-molecule and enzymatic asymmetric catalysis will inform a more sophisticated design of chain-end-controlled radical chemistry for precision macromolecular synthesis. We see that the functional properties of commodity or discovered polymers can be further diversified or improved through tacticity engineering.

Methods

General procedure of Co–por-initiated stereocontrolled LRP

A toluene solution (10.0 ml) of Co^{II}–por (0.01 mmol), AgOTf (0.04 mmol, 10.3 mg), Na_2HPO_4 (0.08 mmol, 11.36 mg) and MeOH (1.0 ml) was degassed through three freeze–pump–thaw cycles and refilled with CO (1 atm). The mixture was then stirred for 7 h under dark at room temperature to generate R–Co^{III}–por. The inorganic impurities were removed by water extraction. The remaining organic solvent was evaporated and followed by addition of acrylamide monomer (4 mmol), a specified amount of LAs and solvent (4 ml). After three freeze–pump–thaw cycles, the flask was refilled with N_2 and irradiated with visible light for 5 h. The polymer product was purified by dialysis against methanol. The monomer conversion and tacticity of polymer were determined by ^{1}H-NMR spectroscopy in DMSO-d_6. The number-average molecular weight and dispersity were determined by GPC with a DMF (0.1 mol l^{-1} LiNTf$_2$) eluent.

Material characterization methods

LCSTs of polyDEAA were measured by a Shimadzu UV-3600Plus or a Unisoku ultraviolet-visible light spectrometer scanned with a programmed temperature profile. Samples were dissolved in H_2O at a concentration of 5 mg ml^{-1} for primary measurements. During each measurement, transmittance of polymer solution was recorded after isothermal equilibration at each temperature for 5 min. The LCST was determined to be the temperature at which 50% transmittance dropped.

Lap shear measurements were conducted on an Instron 5960 tensile testing system. Lap shear stress and strain were recorded at room temperature at an extension speed of 5.0 mm min^{-1}. Purified polyHEAA (1 g) was first dissolved in methanol (10 ml), followed by addition of glycerol (1 g). The mixtures were vigorously stirred until homogenous solutions formed. Methanol was removed under reduced pressure and the resulting mixtures were used for the measurement. Glass slides (8.5 cm × 2.2 cm × 1.5 mm) were directly used without any pretreatment. Both polyHEAA and commercial samples were painted on a 2.2 × 2.0 cm^2 area that was 0.1 mm thick. The adhered interfaces were equilibrated at room temperature for roughly 3 h before testing.

Electrochemical impedance spectroscopy measurements were performed using a Solartron SI 1260 impedance and gain phase analyser. A frequency range of 10^6 to 1 Hz with a polarization amplitude of 20 mV was applied. All samples were fabricated in a nitrogen glovebox. Temperature-dependent ion conductivity was measured from 25 to 80 °C with 30-min equilibration time at each temperature. Polymers were dissolved in acetonitrile (roughly 50 mg ml^{-1}), stirred for approximately 3 h, and drop-casted onto circular stainless-steel discs in the glovebox. A Teflon ring with a thickness of 0.254 mm and an inner diameter of 9.525 mm was used as a spacer to ensure no thickness variation during the measurements. Acetonitrile was slowly evaporated in the glovebox for over 8 h, which produced smooth and homogenous films. The samples were then placed into the vacuum chamber of the glovebox and dried under vacuum for 12 h before testing.

Data availability

All data are available in the main text or the supplementary materials. Source data are provided with this paper.

References

1. Worch, J. C. et al. Stereochemical enhancement of polymer properties. *Nat. Rev. Chem.* **3**, 514–535 (2019).
2. Karasz, F. E. & MacKnight, W. J. The influence of stereoregularity on the glass transition temperatures of vinyl polymers. *Macromolecules* **1**, 537–540 (1968).
3. Pino, P. & Suter, U. W. Some aspects of stereoregulation in the stereospecific polymerization of vinyl monomers. *Polymer* **17**, 977–995 (1976).
4. Uryu, T., Ohkawa, H. & Oshima, R. Synthesis and high hole mobility of isotactic poly(2-*N*-carbazolylethyl acrylate). *Macromolecules* **20**, 712–716 (1987).
5. Wang, Y. et al. Facile synthesis of isotactic polyacrylonitrile via template polymerization in interlayer space for dielectric energy storage. *ACS Appl. Polymer Mat.* **2**, 775–781 (2020).
6. Schurer, J. W., de Boer, A. & Challa, G. Influence of tacticity of poly(methyl methacrylate) on the compatibility with poly(vinyl chloride). *Polymer* **16**, 201–204 (1975).
7. Rajalingam, P. & Radhakrishxan, G. Polyacrylonitrile precursor for carbon fibers. *J. Macromol. Sci. C* **31**, 301–310 (1991).
8. Min, K. E. & Paul, D. R. Effect of tacticity on permeation properties of poly(methyl methacrylate). *J. Polym. Sci., Part B: Polym. Phys.* **26**, 1021–1033 (1988).
9. Yan, M., Lo, J. C., Edwards, J. T. & Baran, P. S. Radicals: reactive intermediates with translational potential. *J. Am. Chem. Soc.* **138**, 12692–12714 (2016).
10. Teator, A. J., Varner, T. P., Knutson, P. C., Sorensen, C. C. & Leibfarth, F. A. 100th Anniversary of macromolecular science viewpoint: the past, present, and future of stereocontrolled vinyl polymerization. *ACS Macro Letters* **9**, 1638–1654 (2020).
11. Coates, G. W. Precise control of polyolefin stereochemistry using single-site metal catalysts. *Chem. Rev.* **100**, 1223–1252 (2000).
12. Chen, E. Y. X. Coordination polymerization of polar vinyl monomers by single-site metal catalysts. *Chem. Rev.* **109**, 5157–5214 (2009).
13. Neuwald, B., Caporaso, L., Cavallo, L. & Mecking, S. Concepts for stereoselective acrylate insertion. *J. Am. Chem. Soc.* **135**, 1026–1036 (2013).
14. Ouchi, M., Kamigaito, M. & Sawamoto, M. Stereoregulation in cationic polymerization by designed Lewis acids. 1. Highly isotactic poly(isobutyl vinyl ether) with titanium-based Lewis acids. *Macromolecules* **32**, 6407–6411 (1999).
15. Teator, A. J. & Leibfarth, F. A. Catalyst-controlled stereoselective cationic polymerization of vinyl ethers. *Science* **363**, 1439 (2019).
16. Satoh, K. & Kamigaito, M. Stereospecific living radical polymerization: dual control of chain length and tacticity for precision polymer synthesis. *Chem. Rev.* **109**, 5120–5156 (2009).
17. Braunecker, W. A. & Matyjaszewski, K. Controlled/living radical polymerization: features, developments, and perspectives. *Prog. Polym. Sci.* **32**, 93–146 (2007).
18. Iizuka, Y. et al. Chiral (–)-DIOP ruthenium complexes for asymmetric radical addition and living radical polymerization reactions. *Eur. J. Org. Chem.* **2007**, 782–791 (2007).
19. Puts, R. D. & Sogah, D. Y. Control of living free-radical polymerization by a new chiral nitroxide and implications for the polymerization mechanism. *Macromolecules* **29**, 3323–3325 (1996).
20. Porter, N. A., Allen, T. R. & Breyer, R. A. Chiral auxiliary control of tacticity in free radical polymerization. *J. Am. Chem. Soc.* **114**, 7676–7683 (1992).
21. Habaue, S. & Okamoto, Y. Stereocontrol in radical polymerization. *Chem. Record* **1**, 46–52 (2001).
22. Paleos, C. M. *Polymerization in Organized Media* (CRC Press, 1992).
23. Isobe, Y., Fujioka, D., Habaue, S. & Okamoto, Y. Efficient Lewis acid-catalyzed stereocontrolled radical polymerization of acrylamides. *J. Am. Chem. Soc.* **123**, 7180–7181 (2001).
24. Bovey, F. Polymer NSR spectroscopy. V. The effect of zinc chloride on the free radical polymerization of methyl methacrylate. *J. Polym. Sci.* **47**, 480–481 (1960).
25. Noble, B. B. & Coote, M. L. in *Advances in Physical Organic Chemistry* Vol. 49 (eds Williams, I. H. & Williams, N. H.) 189–258 (Academic Press, 2015).
26. Zhao, Y., Yu, M. & Fu, X. Photo-cleavage of the cobalt–carbon bond: visible light-induced living radical polymerization mediated by organo-cobalt porphyrins. *Chem. Commun.* **49**, 5186–5188 (2013).
27. Wayland, B. B., Poszmik, G., Mukerjee, S. L. & Fryd, M. Living radical polymerization of acrylates by organocobalt porphyrin complexes. *J. Am. Chem. Soc.* **116**, 7943–7944 (1994).
28. Romain, C., Thevenon, A., Saini, P. K. & Williams, C. K. in *Carbon Dioxide and Organometallics* (ed. Lu, X.-B.) 101–141 (Springer, 2015).
29. Delferro, M. & Marks, T. J. Multinuclear olefin polymerization catalysts. *Chem. Rev.* **111**, 2450–2485 (2011).
30. Wu, Z., Peng, C.-H. & Fu, X. Tacticity control approached by visible-light induced organocobalt-mediated radical polymerization: the synthesis of crystalline poly(*N*,*N*-dimethylacrylamide) with high isotacticity. *Polym. Chem.* **11**, 4387–4395 (2020).
31. Imamura, Y., Fujita, T., Kobayashi, Y. & Yamago, S. Tacticity, molecular weight, and temporal control by lanthanide triflate-catalyzed stereoselective radical polymerization of acrylamides with an organotellurium chain transfer agent. *Polym. Chem.* **11**, 7042–7049 (2020).
32. Shanmugam, S. & Boyer, C. Stereo-, temporal and chemical control through photoactivation of living radical polymerization: synthesis of block and gradient copolymers. *J. Am. Chem. Soc.* **137**, 9988–9999 (2015).
33. Lutz, J.-F., Neugebauer, D. & Matyjaszewski, K. Stereoblock copolymers and tacticity control in controlled/living radical polymerization. *J. Am. Chem. Soc.* **125**, 6986–6993 (2003).
34. Izatt, R. M., Pawlak, K., Bradshaw, J. S. & Bruening, R. L. Thermodynamic and kinetic data for macrocycle interaction with cations, anions, and neutral molecules. *Chem. Rev.* **95**, 2529–2586 (1995).
35. Arnaud-Neu, F., Delgado, R. & Chaves, S. Critical evaluation of stability constants and thermodynamic functions of metal complexes of crown ethers (IUPAC Technical Report). *Pure Appl. Chem.* **75**, 71–102 (2003).
36. Izatt, R. M. et al. Thermodynamic and kinetic data for cation-macrocycle interaction. *Chem. Rev.* **85**, 271–339 (1985).
37. Isobe, Y., Nakano, T. & Okamoto, Y. Stereocontrol during the free-radical polymerization of methacrylates with Lewis acids. *J. Polym. Sci., Part A: Polym. Chem.* **39**, 1463–1471 (2001).
38. Park, B., Imamura, Y. & Yamago, S. Stereocontrolled radical polymerization of acrylamides by ligand-accelerated catalysis. *Polym. J.* **53**, 515–521 (2021).
39. Ray, B. et al. RAFT polymerization of *N*-isopropylacrylamide in the absence and presence of $Y(OTf)_3$: simultaneous control of molecular weight and tacticity. *Macromolecules* **37**, 1702–1710 (2004).
40. Su, X. et al. Stereocontrol during photo-initiated controlled/living radical polymerization of acrylamide in the presence of Lewis acids. *Eur. Polym. J.* **44**, 1849–1856 (2008).
41. Doi, Y. & Asakura, T. Catalytic regulation for isotactic orientation in propylene polymerization with Ziegler-Natta catalyst. *Makromol. Chem. Phys.* **176**, 507–509 (1975).
42. Seliktar, D. Designing cell-compatible hydrogels for biomedical applications. *Science* **336**, 1124–1128 (2012).
43. Zhao, Y. et al. Somatosensory actuator based on stretchable conductive photothermally responsive hydrogel. *Sci. Robotics* **6**, eabd5483 (2021).

44. Liu, H. & Zhu, X. Lower critical solution temperatures of N-substituted acrylamide copolymers in aqueous solutions. *Polymer* **40**, 6985–6990 (1999).
45. Ou, W. et al. In-situ cryo-immune engineering of tumor microenvironment with cold-responsive nanotechnology for cancer immunotherapy. *Nat. Commun.* **14**, 392 (2023).
46. Pantula, A. et al. Untethered unidirectionally crawling gels driven by asymmetry in contact forces. *Sci. Robotics* **7**, eadd2903 (2022).
47. Zhao, D., Wang, P., Zhao, Q., Chen, N. & Lu, X. Thermoresponsive copolymer-based draw solution for seawater desalination in a combined process of forward osmosis and membrane distillation. *Desalination* **348**, 26–32 (2014).
48. Tsuchiizu, A., Hasegawa, T. & Katsumoto, Y. Water sorption on a thin film of stereocontrolled poly(*N*-ethylacrylamide) and poly(*N*,*N*-diethylacrylamide). In *Proc. ICOMF14 – 14th International Conference on Organized Molecular Films (LB 14)*, MATEC Web of Conferences, 03001 (EDP Sciences, 2013).
49. Rzaev, Z. M. O., Dinçer, S. & Pişkin, E. Functional copolymers of *N*-isopropylacrylamide for bioengineering applications. *Prog. Polym. Sci.* **32**, 534–595 (2007).
50. Pang, X. & Cui, S. Single-chain mechanics of poly(*N*,*N*-diethyl-acrylamide) and poly(*N*-isopropylacrylamide): comparative study reveals the effect of hydrogen bond donors. *Langmuir* **29**, 12176–12182 (2013).
51. Katsumoto, Y., Kubosaki, N. & Miyata, T. Molecular approach to understand the tacticity effects on the hydrophilicity of poly(*N*-isopropylacrylamide): solubility of dimer model compounds in water. *J. Phys. Chem. B* **114**, 13312–13318 (2010).
52. Wirthl, D. et al. Instant tough bonding of hydrogels for soft machines and electronics. *Sci. Adv.* **3**, e1700053 (2017).
53. Li, J. et al. Tough adhesives for diverse wet surfaces. *Science* **357**, 378–381 (2017).
54. Cui, C. & Liu, W. Recent advances in wet adhesives: adhesion mechanism, design principle and applications. *Prog. Polym. Sci.* **116**, 101388 (2021).
55. Larcher, D. & Tarascon, J. M. Towards greener and more sustainable batteries for electrical energy storage. *Nat. Chem.* **7**, 19–29 (2015).
56. Kim, H. J., Chen, B., Suo, Z. & Hayward, R. C. Ionoelastomer junctions between polymer networks of fixed anions and cations. *Science* **367**, 773–776 (2020).
57. Gao, D. & Lee, P. S. Rectifying ionic current with ionoelastomers. *Science* **367**, 735–736 (2020).
58. Lopez, J., Mackanic, D. G., Cui, Y. & Bao, Z. Designing polymers for advanced battery chemistries. *Nat. Rev. Materials* **4**, 312–330 (2019).
59. Choi, U. H. et al. Ionic conduction and dielectric response of poly(imidazolium acrylate) ionomers. *Macromolecules* **45**, 3974–3985 (2012).
60. Weiber, E. A. & Jannasch, P. Ion distribution in quaternary-ammonium-functionalized aromatic polymers: effects on the ionic clustering and conductivity of anion-exchange membranes. *Chem. Sus. Chem.* **7**, 2621–2630 (2014).

Acknowledgements

This project was financially supported by United States National Science Foundation (grant no. CHE-2108681). M.Z. acknowledges the support through a 3M Non-Tenured Faculty Award. J.M. Mayer and E. Stewart-Jones are acknowledged for their assistance with the variable-temperature ultraviolet-visible light measurements. We thank P. Guo for light intensity measurement, J. Yan for providing access to a cold room to carry out low-temperature polymerizations, and A. Datye and Y. Xue for help with the thermomechanical tests. We acknowledge N. Hazari, S.J. Miller, S. Lin, K. Kawamoto, Y. Gu, J. Zhao, A.N. Le and Y. Ma for helpful discussions.

Author contributions

M.Z., X.Z. and F.L. designed the research. X.Z., F.L. and M.C. conducted the experiments. M.Z., X.Z. and M.C. wrote the manuscript with input from F.L.

Competing interests

X.Z. and M.Z. are inventors on a patent application (US provisional patent application no. 63/427,662) submitted by Yale University that covers the development of catalysts/initiators for stereocontrolled living polymerizations and of related tacticity-engineered functional polymers. The remaining authors declare no competing interests.

Additional information

Supplementary information The online version contains supplementary material available at https://doi.org/10.1038/s44160-023-00311-9.

Correspondence and requests for materials should be addressed to Mingjiang Zhong.

Peer review information *Nature Synthesis* thanks Shigeru Yamago and the other, anonymous, reviewer(s) for their contribution to the peer review of this work. Primary Handling Editor: Alison Stoddart, in collaboration with the *Nature Synthesis* team.